ARTICLE NO. 79-0674R

Diagnostic Evaluation of Jet Noise Suppression Mechanisms

P. R. Gliebe*
General Electric Company, Cincinnati, Ohio

A unified aeroacoustic jet noise prediction method has been developed based on the modeling of principal noise generation and emission mechanisms from first principles. It is demonstrated herein that this jet noise prediction method is a useful diagnostic tool for assessing the relative importance of the various mechanisms for a given nozzle type. The relative contributions of 1) turbulent mixing noise suppression, 2) shock-cell broadband noise suppression, 3) convective amplification suppression, and 4) fluid shielding attenuation have been evaluated for a high element number multichute suppressor to arrive at a plausible explanation for how multielement suppressors suppress jet noise. This explanation, an alternative view to historical conceptions of jet noise suppression, suggests an approach to designing low noise suppressor nozzles.

Nomenclature

A	= nozzle exhaust area, m^2
AR	= suppressor area ratio; ratio of total nozzle area (excluding plug) to flow area
D	= diameter, m
f	= 1/3 octave frequency, Hz
F_s	= ideal gross static thrust, N
PNL	= perceived noise level, PNdB
SPL	= sound pressure level, dB (referenced to 0.0002 dynes/cm^2)
OASPL	= overall sound pressure level, dB
T	= temperature, K
V	= jet flow velocity, m/s
Θ_i	= observer angle, deg (relative to inlet axis)
ρ	= jet flow density, Kg/m^3
ω	= density ratio exponent (per SAE ARP 876)

Subscripts

a	= ambient or aircraft conditions
eq	= equivalent dimension based on total flow area
i	= inner stream
j	= jet exit plane fully-expanded value
ma	= mass-averaged condition
o	= outer stream
p	= peak value
T	= total or stagnation value

Introduction

As part of an extensive research program on high velocity jet noise reduction, several basic theoretical studies and critical experiments were conducted, documented in Ref. 1. The purpose of these basic studies and experiments was to identify and quantify the important jet noise generation and emission mechanisms. From these studies and experiments, a unified aeroacoustic jet noise prediction method was developed, based on a modeling of the principal noise generation and emission mechanisms from first principles, rather than utilizing empirical correlations of experimental results. This unified aeroacoustic prediction computer model is described in detail in Refs. 1 and 2.

Presented as Paper 79-0674 at the AIAA 5th Aeroacoustics Conference, Seattle, Wash., March 12-14, 1979; submitted April 25, 1979; revision received March 20, 1980.

Index categories: Noise; Aeroacoustics.

*Manager, Aeroacoustic Analysis and Prediction Development, Aircraft Engine Group. Member AIAA.

Extensive data/theory comparisons were carried out, for a wide variety of nozzle types and operating conditions, in order to verify the jet noise principles upon which the prediction model is based. The emphasis was placed on the ability to predict full-size engine nozzle jet noise at typical engine takeoff and sideline conditions. The many data/theory comparisons carried out showed that the prediction model was capable of predicting the acoustic characteristics of jets of most any type.

It is demonstrated herein that the unified prediction model is a useful diagnostic tool for assessing the relative importance of the various jet noise mechanisms for a given nozzle type, and can serve as a design evaluation and optimization tool. The relative contributions of: 1) mixing noise suppression, 2) shock-cell broadband noise suppression, 3) convective amplification suppression, and 4) fluid shielding attenuation, have been evaluated for a high element number multichute suppressor. These diagnostic computations with the unified aerodynamic prediction model have been analyzed to arrive at a plausible explanation for how and why multielement jet nozzles suppress jet noise.

Prediction Model Description

The unified aeroacoustic prediction model for the noise of arbitrary jets is based on four primary sound emission mechanisms: 1) sound generation by the turbulence produced in the mixing zones of the jet plume, convecting with the flow; 2) convective amplification due to turbulent eddy motion relative to the observer; 3) mean-flow shrouding (fluid shielding) of the generated sound; and 4) shock cell broadband noise. The prediction model contains four major elements: 1) an aerodynamic flowfield prediction procedure, 2) a sound-flow interaction acoustic model, 3) a mixing noise source spectrum model, and 4) a shock cell noise prediction. These four elements are described briefly in the following paragraphs. A detailed description can be found in Refs. 1 and 2.

The aerodynamic flowfield is modeled using an extension of Reichardt's theory.[4,5] Because the governing equations for diffusion of momentum and enthalpy are linear, the summation of elemental solutions is also a solution. The superposition feature of Reichardt's method permits the construction of quite complex jet flowfields with relatively simple and rapid computational techniques. This flow modeling approach has been applied to coannular jet flows by Balsa and Gliebe.[6,7]

The sound-flow interaction effects are modeled using analytical expressions for the far field sound pressure

produced by convecting sources imbedded in a parallel shear flow jet developed by Balsa.[3] The solutions require a description of the velocity and temperature profiles in the jet, provided by the aerodynamic model.

The aerodynamic prediction model also provides predictions of the characteristic strength, frequency, and size of the convecting sources throughout the jet plume. The characteristic frequency and length scale are determined from the aerodynamic predictions of mean and turbulent velocities utilizing the empirical similarity relations of Davies et al.[8] The shock cell noise is modeled using a modification of the procedure developed by Harper-Bourne and Fisher.[9]

The above analytical model elements have been integrated into a unified computational procedure. The jet plume is subdivided into elemental "eddy" volumes, each having its own source strength, spectrum and flow shrouding, as illustrated in Fig. 1. The simple closed-form acoustic pressure solutions, combined with the simple aerodynamic calculation method, permits rapid, economical computations of the entire jet plume aerodynamic and acoustic characteristics, including far field spectra at all observer angles. The contributions from each elemental jet volume are simply added on a mean-square pressure basis, in each frequency band. The shock cell noise contribution is then computed separately and added to the mixing noise contribution to yield the total far field spectra.

Theory/Data Comparisons

An extensive data/theory comparison study was carried out to verify the jet noise suppression mechanisms identified in Ref. 1. The aeroacoustic jet noise prediction model was used to predict the acoustic characteristics of seven nozzle configurations at several operating points for each configuration. These predictions were compared to the experimental data obtained from scale-model tests and engine tests. Comparisons were made of perceived noise level (PNL) vs jet exhaust velocity, PNL directivity, and one-third octave sound pressure level spectra at selected observed angles.

The approach taken was to compare predicted and measured noise characteristics on the basis of full-scale engine subjective noise levels (PNL), using a total exhaust flow area of $A_T = 0.218$ m^2 (338 in.^{2}) at a sideline distance of 731.5 m (2400 ft). Details of the data/theory comparisons are given in Ref. 10. Only the conical and multichute nozzle comparisons are presented herein.

Results are presented in terms of perceived noise level, PNL, normalized according to the relationship

$$\mathrm{PNL}_N = \mathrm{PNL} - 10\log_{10}[F_S(T_a/T_{ma})^{\omega-1}]$$

where F_s = static, ideal gross thrust, T_a = ambient temperature, T_{ma} = static temperature corresponding to mass-averaged velocity and total temperature at nozzle exit plane, and ω = jet density exponent (per SAE ARP876) based on mass-averaged velocity V_{ma}.

Figure 2 shows the comparison of experimental and predicted peak PNL_N vs V_{ma} trends for a conical nozzle. The predicted levels are seen to be within the data band throughout the jet velocity range. A comparison of predicted PNL_N vs V_{ma} characteristics for a 36-element, single-flow chute suppressor nozzle is shown in Fig. 3. The characteristics are seen to be much flatter than those for the conical nozzle shown in Fig. 2. The fact that both conical-nozzle and chute-nozzle PNL_N characteristics are predicted accurately implies that PNL suppression is also predicted reasonably well.

The results for a 36-chute suppressed-fan dual-flow nozzle are shown in Fig. 4. Again, it is observed that the PNL_N vs V_{ma} trends are well predicted by the aeroacoustic model. It is encouraging (and important) that the characteristics of a multielement, dual-stream system can be accurately predicted since it is this type of system that is currently envisioned for future SCAR (Supersonic Cruise Airplane Research) engine designs. Examples of predicted vs measured PNL directivity patterns for a conical and a multichute nozzle are shown in Figs. 5 and 6. These examples demonstrate reasonably good agreement between prediction and data. Sample comparisons of predicted and measured SPL spectra for the multichute turbojet suppressor are shown in Fig. 7. The characteristic flat spectrum shape exhibited by multichute nozzles is well predicted by the theoretical model.

To evaluate the ability of the aeroacoustic model to predict the effects of chute area ratio, predictions were made at several jet velocities for suppressor nozzles having area ratios of 1.5, 2.0, and 2.5. A summary of these predicted and measured results is shown in Fig. 8, where peak PNL suppression (relative to an equivalent-thrust, conical nozzle) is plotted vs jet velocity. The predicted points are denoted by symbols; the data has been curve-fitted, and the corresponding lines are shown. These results show that a suppression peak can be predicted; i.e., suppression is *not* constant with varying V_j, has a definite maximum at some

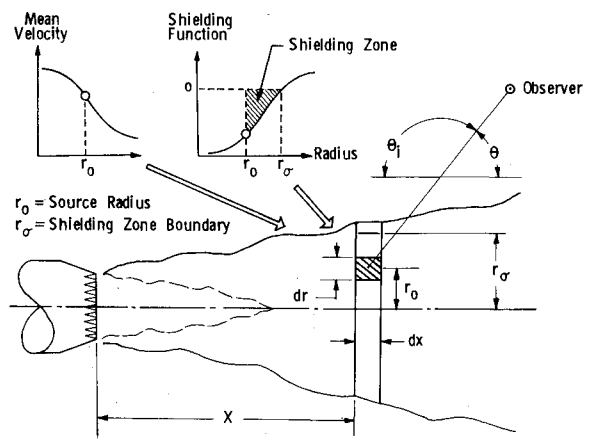

Fig. 1 Generalized volume element model.

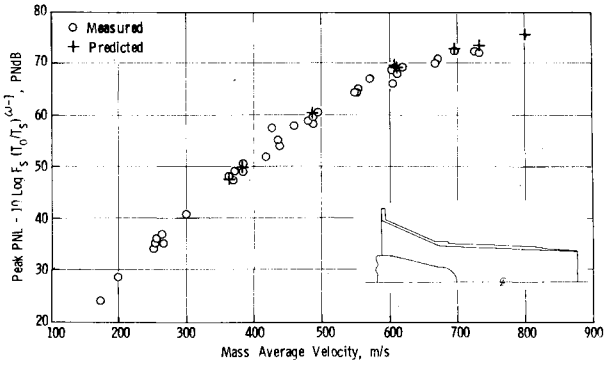

Fig. 2 Predicted vs measured normalized PNL for a conical nozzle.

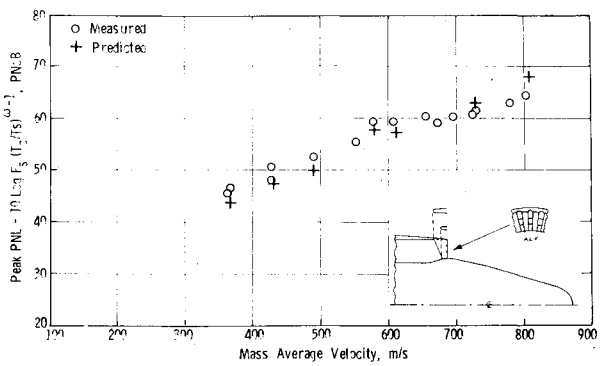

Fig. 3 Predicted vs measured normalized PNL for a 36 chute, $AR = 2.0$ turbojet suppressor nozzle.

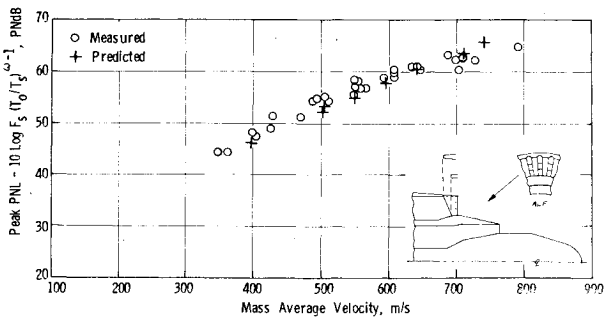

Fig. 4 Predicted vs measured normalized PNL for a 36 chute, $AR = 2.0$, $A_o/A_i = 1.92$ dual flow suppressor nozzle.

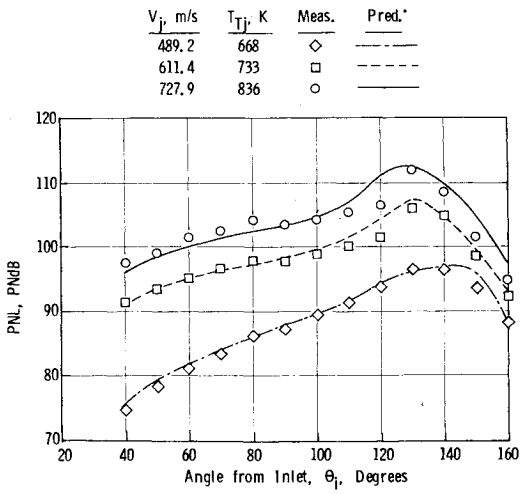

Fig. 5 Predicted vs measured PNL directivity for a conical nozzle.

value of V_j, and falls off with decreasing and increasing V_j on either side of the peak. Although the predicted suppression curve (circles) deviates from the data (solid line) at low velocities, the general trend and curve shapes are consistent.

Diagnostic Evaluation of Noise Mechanisms

A thorough discussion of jet noise generation and emission mechanisms has been presented elsewhere.[1] The objective of the present discussion is to identify the relative roles these mechanisms play in the suppression of jet noise. These mechanisms are as follows: 1) turbulent mixing noise generation, 2) convective amplification, 3) fluid shielding, and 4) shock-cell broadband noise. The preceding section has shown that the present mathematical model representation of these mechanisms (collectively) yields a fairly accurate prediction of the far-field acoustic characteristics of turbulent jets, for a wide variety of shapes and flow conditions. It is therefore of interest to evaluate how the individual mechanisms combine to yield the far-field result; and more importantly, how these mechanisms change due to the addition of a suppressor to a baseline nozzle.

A parametric study was performed to evaluate the relative contributions of the above four mechanisms to the far-field noise for both a baseline conical nozzle and a typical high-suppression, multielement nozzle. The 36-chute, AR = 2.0 turbojet suppressor was chosen for this study as representative of a high-element number, high-suppression (10-12 PNdB) exhaust system. A typical takeoff condition of V_j = 731.5 m/s (2400 ft/s) and T_{T_j} = 905.6 K (1630°R) was selected for evaluation. Both the baseline conical nozzle and the 36-chute suppressor nozzle exit areas were 0.218 m^2 (338 $in.^2$). Noise characteristics were evaluated on a 731.5 m (2400 ft) sideline.

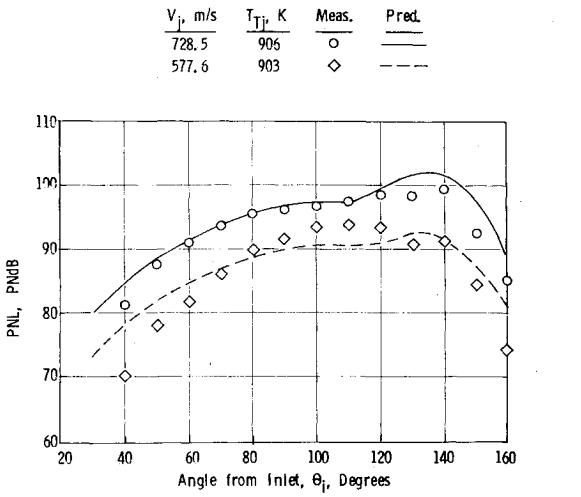

Fig. 6 Predicted vs measured PNL directivity for a 36 chute, $AR = 2.0$ turbojet suppressor nozzle.

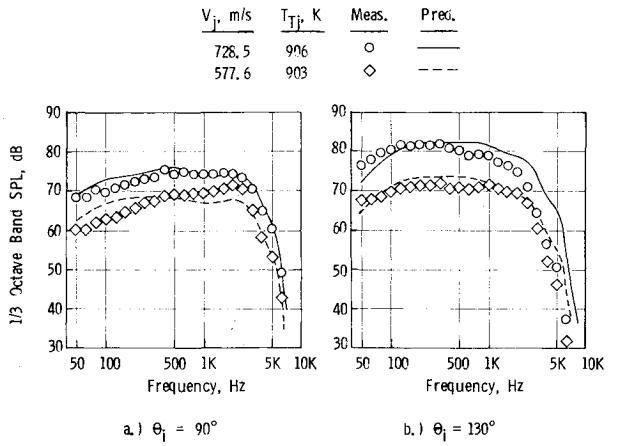

Fig. 7 Predicted vs measured SPL spectra for a 36 chute, $AR = 2.0$ turbojet suppressor nozzle.

The computations were performed in four modes, as follows: a) Complete acoustic calculation; b) As in a), but shock-cell noise omitted; c) As in b), but fluid shielding omitted; and d) As in c), but convective amplification omitted. For the chute suppressor, mode a was omitted since the ability to model multichute nozzle shock-cell noise is not yet established. The difference in noise levels between modes a) and b) is a measure of the shock-cell noise contribution to the total jet noise signature. The difference in noise levels between modes b) and c) is a measure of the influence of fluid shielding on the jet noise. Finally, the difference in levels between modes c) and d) indicates the amount of convective amplification that is present in the jet.

The results of the above series of computations are summarized in Figs. 9-11. Figure 9 shows the PNL directivity patterns for the different prediction modes. Also shown are the measured data for reference, which should be compared with mode a) predictions (mode b for the chute nozzle). Figures 10 and 11 display the corresponding spectrum shapes (1/3 octave SPL) at Θ_i = 50 deg and 130 deg respectively. The measured spectra are also shown for reference. Considering the conical nozzle PNL directivity patterns, Fig. 9, it is observed that shock-cell noise contributes substantially to the total noise in the forward quadrant, $\Theta_i < 90$ deg. This can be seen by noting the difference between mode a) and mode b) predictions. There is no contribution of shock noise close to the jet axis ($\Theta_i > 120$ deg) because mode a) and b) predictions are identical in this region. There is no fluid shielding for observer angles less than about 110 deg based on comparing

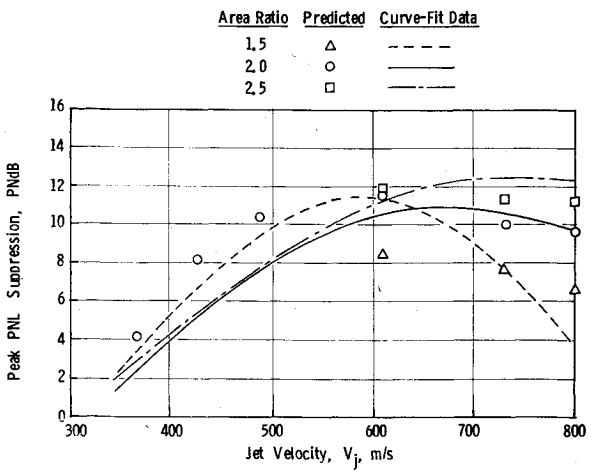

Fig. 8 Predicted vs measured effect of area ratio on peak PNL suppression for a 36 chute turbojet suppressor nozzle.

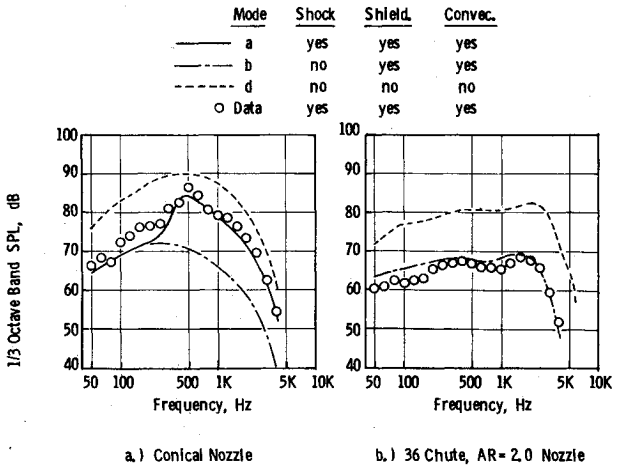

Fig. 10 Relative contribution of noise mechanisms to SPL spectra at $\Theta_i = 50$ deg for a conical nozzle and 36 chute, $AR = 2.0$ nozzle at $V_j = 731.5$ m/s.

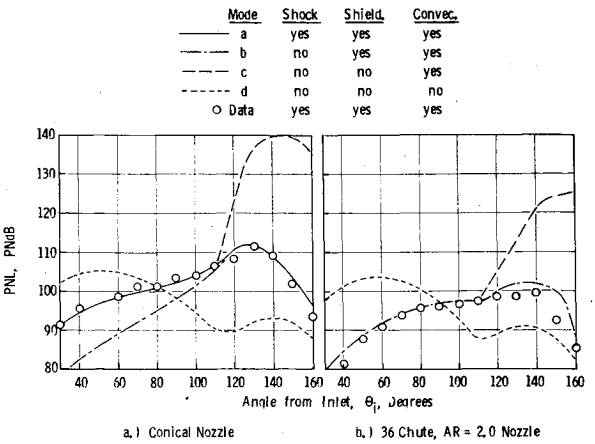

Fig. 9 Relative contribution of noise mechanisms to PNL directivity at $V_j = 731.5$ m/s.

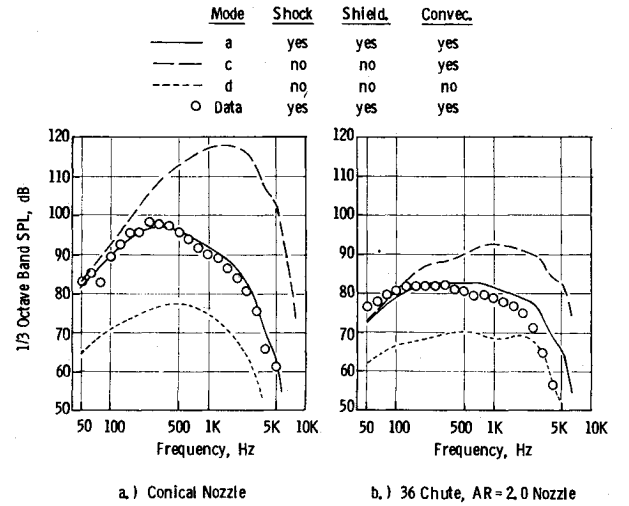

Fig. 11 Relative contribution of noise mechanisms to SPL spectra at $\Theta_i = 130$ deg for a conical nozzle and 36 chute, $AR = 2.0$ nozzle at $V_j = 731.5$ m/s.

mode b) and c) predictions. For $\Theta_i > 110$ deg, however, shielding effects become quite substantial, on the order of 30 PNdB. Eddy-convection effects are also large; they increase the noise in the aft quadrant ($\Theta_i > 90$ deg). This effect is apparent from comparing mode c) and d) predictions.

The mode d) prediction shown in Fig. 9a represents the basic turbulent-mixing noise in the absence of convection and fluid-shielding effects. It possesses a basic, nonconstant directivity pattern dictated by the weighted summation of various quadrupole types composing the turbulent eddies. This basic pattern is only symmetric about $\Theta_i = 90$ deg when the local flow Mach number is zero because the quadrupole weighting factors are a function of local Mach number and bias the radiation toward the forward quadrant.[3]

The corresponding PNL directivity patterns for the 36-chute suppressor are shown in Fig. 9b. The trends discussed above for the conical nozzle are qualitatively similar for the 36-chute nozzle, with the exception of the shock-cell noise contribution. The predictions were made neglecting shock-cell noise (mode b), and yet the predictions agree with the data, as Fig. 9 shows. This implies that shock-cell noise is not a significant feature of multichute nozzles. It also appears that neither convection effects nor fluid-shielding effects are as strong as for the conical nozzle.

The breakdown of mechanisms for a typical forward-quadrant angle of $\Theta_i = 50$ deg is shown in Fig. 10. No shielding occurs at this angle; therefore the mode c) results are omitted, as they are identical to the mode b) results. The conical nozzle results, Fig. 10a, show an interesting counteraction among the mechanisms. The basic mixing-noise spectrum, mode d) yields a high noise level, much higher than the measured level. The convection effect is to Doppler-shift and drop this spectrum to a level significantly lower than the data (except at very low frequencies), as indicated by the mode b) prediction. Finally, the addition of the shock-cell noise spectrum raises the spectrum back up to the measured level at middle-to-high frequencies.

The corresponding 36-chute 50 deg spectrum results are shown in Fig. 10b. The good agreement between the mode b) spectrum prediction and the measured spectrum substantiates the implication drawn from Fig. 9b. Shock-cell noise may not be a significant source for multichute suppressors. Again the effect of convection is to reduce the level and Doppler-shift the spectrum to lower frequencies. Fluid-shielding effects are absent at 90 deg, and convection effects are less than 0.5 dB throughout the frequency range. The shock-cell noise was not computed for the chute nozzle; thus, the only significant contribution at 90 deg for the chute nozzle is the basic mixing-noise spectrum (Fig. 7).

Near the peak-noise angle, $\Theta_i = 130$ deg, convection effects again become significant. They produce a dramatic amplification of the mixing noise, as the results in Fig. 11 show. Another counter-action of mechanisms occurs at this angle, involving the competing effects of convection and fluid shielding. The basic mixing-noise spectrum is much lower than the measured level, as shown in Fig. 11a, mode d). The

effect of convection is to increase the levels by as much as 40-50 dB at high frequencies. The effect of shielding, however, is to reduce the noise levels by 20 to 30 dB at high frequencies, such that the net noise levels agree with the measured levels.

It is interesting to note that the convection effect Doppler-shifts the basic mixing-noise spectrum to higher frequencies, as would be expected from classical notions of moving-source acoustics. However, the fluid-shielding effects, which increase with increasing frequency, attenuate the high-frequency portion of the convected spectrum to such a large extent that the resulting spectrum peaks at a much lower fequency, lower than even the basic unconvected spectrum peak. This explains the observed "reverse Doppler shift" at angles close to the jet axis.

The competing influences of convection and fluid shielding are also evident in the 36-chute nozzle predictions shown in Fig. 11b. The magnitudes of these effects are considerably smaller than those exhibited by the conical nozzle. For example, at 2000 Hz, the convective amplification is 22 dB for the chute nozzle, compared to 48 dB for the conical nozzle at the same frequency. Similarly, the fluid-shielding attenuation is only 12 dB at 2000 Hz for the chute nozzle, compared to 31 dB attenuation for the conical nozzle.

Discussion of Suppression Mechanisms

The various mechanisms can be isolated explicitly by examining the difference between the various prediction curves shown in Figs. 9 through 11. First, the total PNL suppression as a function of Θ_i is the difference between the conical and chute nozzle total noise PNL directivity patterns. This can be compared with measured PNL suppression and is shown in Fig. 12. The pedicted total PNL suppression is seen to compare well with the measured suppression.

From the results given in Figs. 9-11, it can be concluded that the multichute nozzle almost completely suppresses the shock-cell noise so as to permit the mixing noise to dominate the forward-quadrant spectra. The shock-noise suppression is then approximated by the difference between mode a) and mode b) conical-nozzle predictions. This estimated shock-cell noise suppression is also shown in Fig. 12. The shock-cell noise suppression is seen to be higher than the total predicted suppression in the forward quadrant; hence, some other mechanism is providing negative suppression, i.e., is increasing the PNL.

The suppression of convective amplification can be computed by first calculating the convective amplification for each nozzle, PNL (c)-PNL (d), and then subtracting the chute-nozzle result from the conical-nozzle result. The convective-amplification suppression is shown in Fig. 12. Note that it is negative in the forward quadrant; this explains why the shock-noise suppression is greater than the total (net) suppression.

In a similar fashion, the difference between conical-nozzle fluid-shielding attenuation and 36-chute suppressor fluid-shielding attenuation has been computed from the results shown in Fig. 9, and this difference is shown in Fig. 12. From this result, it is apparent that a multi-element suppressor exhibits reduced fluid-shielding effects relative to a conical nozzle; i.e., part of the beneficial effect of fluid shielding is lost by the addition of a suppressor.

The observed suppression in the aft quadrant is primarily a result of reduced convective amplification, offset somewhat by a loss in fluid shielding. This delicate balance between convection and shielding effects in the aft quadrant is very difficult to predict accurately because these two effects are of large magnitude but opposite in sign, as is illustrated in Fig. 11.

Finally, the suppression of basic turbulent-mixing noise generation has been evaluated by subtracting the mode d) prediction for the chute nozzle from the conical-nozzle mode d) prediction, also shown in Fig. 12. The basic mixing-noise suppression is seen to be quite small, from 1 to 5 dB over the range of angles shown, which is contrary to historical conceptions of how multielement suppressors suppress jet noise.

The multichute suppressor in fact generates approximately the same total mixing noise as the equivalent conical nozzle but redistributes the noise to higher frequencies. This is dramatically illustrated in Fig. 13, where the basic mixing-noise spectra (mode d computations) for the two nozzles are compared. Also shown are these same spectra with the atmospheric (air) attenuation removed, i.e., the lossless spectra. The multichute lossless spectrum is seen to have about the same peak level as the conical-nozzle lossless spectrum, but at a much higher frequency. The ratio of chute-nozzle peak-noise (lossless) frequency to conical-nozzle peak-noise (lossless) frequency is about 6:1. This is precisely the ratio of conical-nozzle diameter to chute-element equivalent-area diameter.

The reduction in shock-cell noise produced by a multichute suppressor can be explained by the fact that breaking up a large, round jet into very small, discrete, rectangular jets will cause the shock-cell formation to be dissipated much more rapidly. The shock-cell spacings and cross-sectional dimensions will be much smaller, and the cells are likely to be fewer in number. The resulting broadband radiation is therefore likely to be much lower in level and higher in frequency than that for a conical nozzle.

The observation that the total generated mixing noise is not significantly different for a multichute suppressor is explained by the fact that the chute-nozzle mixing-layer perimeter close to the nozzle exit plane is considerably larger than an

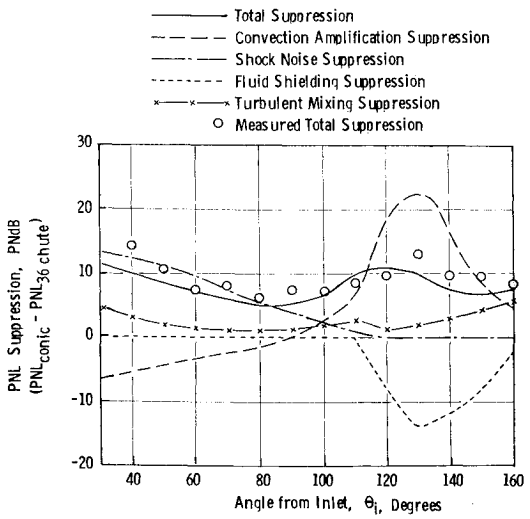

Fig. 12 PNL suppression composition for a 36 chute, $AR = 2.0$ suppressor nozzle at $V_j = 731.5$ m/s.

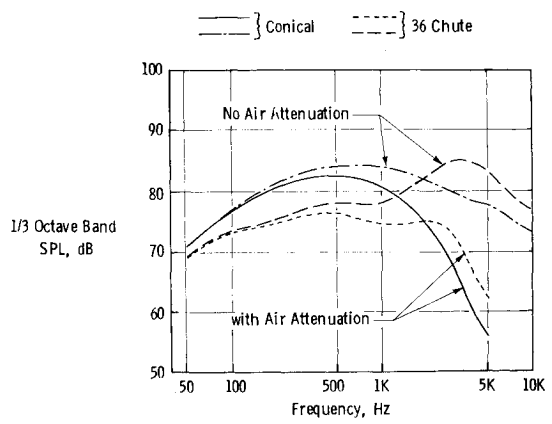

Fig. 13 Comparison of predicted turbulent-mixing noise spectra at $\Theta_i = 90$ deg for a conical nozzle and 36 chute, $AR = 2.0$ nozzle at $V_j = 731.5$ m/s.

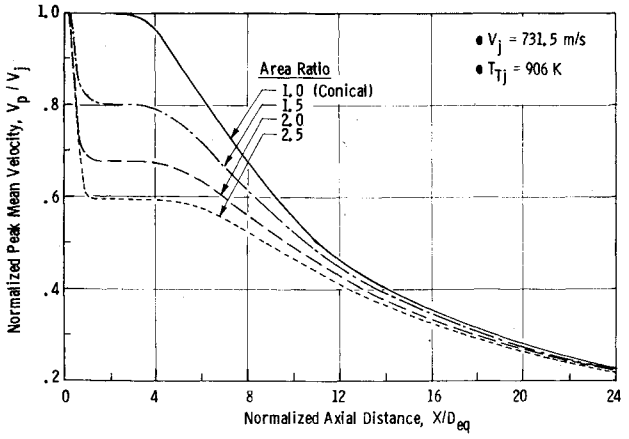

Fig. 14 Predicted mean-velocity axial decay rates for a 36 chute nozzle at $V_j = 731.5$ m/s and $T_{T_j} = 906$ K.

equivalent-area, conical-nozzle perimeter. The high-frequency noise generated in the initial shear layers should therefore be higher by the ratio of perimeters, provided the premerged portion of the chute mixing layers have approximately the same turbulence characteristics. Once the chutes have merged, a large axisymmetric jet forms which has a substantially lower velocity than the exit value; therefore, the low-frequency noise levels should be lower than the corresponding conical-nozzle levels.

The reduction in convection effects exhibited by a multichute nozzle is the result of lower eddy-convection velocities. The rapid plume mean velocity decay exhibited by a multichute nozzle suggests that the majority of the noise-producing turbulent eddies in the plume are convecting downstream at a substantially lower velocity than in a conical nozzle.

The reduced fluid-shielding effects characteristic of a multichute nozzle can also be related to the rapid plume velocity (and temperature) decay. Fluid shielding increases with increasing plume flow velocity and temperature; therefore, the lower velocity and temperature levels resulting from the rapid chute-element mixing provide less fluid shielding than an equivalent-area conical nozzle.

From the above discussion, it can be concluded that the best suppression is achieved by producing the most rapid plume decay. This conclusion is supported by the area-ratio study results shown in Fig. 8, discussed in the previous section. The effect of chute area ratio (at high jet velocities) is to reduce the noise as area ratio is increased. The predicted peak axial mean velocity decay for the three area ratios examined is shown in Fig. 14. The effect of increasing area ratio is to produce more rapid plume decay, in concert with the improved noise suppression.

In the above studies, the effects of base pressure variations on nozzle plume aerodynamics and acoustic characteristics have been ignored. It is suspected that multielement nozzles (e.g., the 36-chute $AR = 1.5$ turbojet nozzle) with area ratios less than two have significant base-pressure reduction (relative to ambient).

In viewing all of the mean-velocity-decay predictions as a whole, the prediction model appears to give the correct trends, i.e., the higher element-number and area-ratio nozzles give more rapid decay. Area ratio controls the merged velocity level plateau; higher area ratios yield lower merged velocity levels. Element number controls how fast the merged-velocity level is reached; higher element numbers give more rapid decay to the merged-velocity level.

Conclusions

The prediction model developed in Ref. 1 provides a reasonably accurate prediction of the acoustic characteristics of suppressor nozzles. It is capable of discerning the effects of suppressor area ratio and element number and shape on the subjective noise levels (PNL) for high velocity jets. The suppression characteristics of multielement nozzles can be explained by means of the four physical mechanisms upon which the prediction is based. It is concluded that multielement suppressors do not substantially reduce the turbulent-mixing-noise generation but, instead, redistribute this noise to higher frequencies where atmospheric (air) attenuation can mitigate the effects on the observer more easily. In the forward quadrant, the major effect of a multielement nozzle is to substantially reduce shock-cell broadband noise radiation. In the aft quadrant, substantial suppression is achieved by a reduction in convective amplification effects. This reduction is offset somewhat by an accompanying loss in fluid shielding suppression, but (for a "good" suppressor) the net effect is still a substantial noise reduction.

Acknowledgements

The work reported herein was carried out for the Federal Aviation Administration under contract FAA/DOT OS-30034 (Task 3). The author is grateful to E.J. Stringas, J.F. Brausch, and W.S. Clapper for their encouragement and guidance while performing the present study, and to the General Electric Company for granting permission to publish this study.

References

[1] Mani, R., and Stringas, E.J., "High Velocity Jet Noise Source Location and Reduction - Task 2 - Theoretical Developments and Basic Experiments," General Electric Company Contractor Report FAA-RD-76-79, II, May 1978.

[2] Gliebe, P.R., "High Velocity Jet Noise Source Location and Reduction - Task 2 Supplement – Computer Program for Calculating the Aeroacoustic Characteristics of Jets from Nozzles of Arbitrary Shape," General Electric Company Contractor Report FAA-RD-76-79, IIa, May 1978.

[3] Balsa, T.F., "The Far Field of High Frequency Convected Singularities in Sheared Flows, with Application to Jet Noise Prediction," *Journal of Fluid Mechanics,* Vol. 74, Pt. 2, March 1976, pp. 193-208.

[4] Reichardt, H., "New Theory of Free Turbulence, *Royal Aeronautical Society Journal,* Vol. 47, 1943, pp. 167-196.

[5] Alexander, L.G., Baron, T., and Comings, W., "Transport of Momentum, Mass and Heat in Turbulent Jets, "University of Illinois Engineering Bulletin No. 413, May 1953.

[6] Balsa, T.F. and Gliebe, P.R., "The Aerodynamics and Noise of Coaxial Jets," *AIAA Journal,* Vol. 15, Nov., 1977, pp. 1550-1558.

[7] Gliebe, P.R., and Balsa, T.F., "Aeroacoustics of Axisymmetric Single and Dual Flow Exhaust Nozzles," *Journal of Aircraft,* Vol. 15, Nov. 1978, pp. 743-749.

[8] Daves, P.O.A.L., Fisher, M.J., and Barratt, M.J., "The Characteristics of the Turbulence in the Mixing Region of a Round Jet," *Journal of Fluid Mechanics,* Vol. 15, March 1963, pp. 337-367.

[9] Harper-Bourne, M. and Fisher, M.J., "The Noise from Shock Waves in Supersonic Jets, "NATO, AGARD Conference Paper CPP-131, 1973.

[10] Clapper, W.S., Gliebe, P.R., Motsinger, R., Sieckman, A., and Stringas, E.J., "High Velocity Jet Noise Source Location and Suppression Task 3 - Experimental Investigation of Suppression Principles, Vol. I," General Electric Contractor Report FAA-RD-76-79, III-I, Dec. 1978.